ADVANCED BIOLOGY
www.advanced-bio.com

Hydrogenated Graphene Improves Neuronal Network Maturation and Excitatory Transmission

Matteo Moschetta, Jong-Young Lee, João Rodrigues, Alice Podestà, Omar Varvicchio, Jangyup Son, Yangjin Lee, Kwanpyo Kim, Gwan-Hyoung Lee, Fabio Benfenati, Mattia Bramini, and Andrea Capasso**

Graphene is regarded as a viable bio-interface for neuroscience due to its biocompatibility and electrical conductivity, which would contribute to efficient neuronal network signaling. Here, monolayer graphene grown via chemical vapor deposition is treated with remote hydrogen plasma to demonstrate that hydrogenated graphene (HGr) fosters improved cell-to-cell communication with respect to pristine graphene in primary cortical neurons. When transferred to polyethylene terephthalate, HGr exhibits higher wettability than graphene (water contact angle of 83.7° vs 40.7°), while preserving electrical conductivity (≈3 kΩ $\square^{-1}$). A rich and mature network is observed to develop onto HGr. The intrinsic excitability and firing properties of neurons plated onto HGr appears unaltered, while the basic passive and active membrane properties are fully preserved. The formation of excitatory synaptic connections increases in HGr with respect to pristine graphene, leading to a doubled miniature excitatory postsynaptic current frequency. This study supports the use of hydrogenation for tailoring graphene into an improved neuronal interface, indicating that wettability, more than electrical conductivity, is the key parameter to be controlled. The use of HGr can bring about a deeper understanding of neuronal behavior on artificial bio-interfaces and provide new insight for graphene-based biomedical applications.

1. Introduction

Traditional treatments for central nervous system disorders have shown limits and challenges.[1–3] Alternative ways to outperform current state-of-the-art technologies are required in neuroscience, especially for neuronal regeneration[4,5] and electrical sensing/recording.[6] Despite a lot of efforts have been made to develop implantable neuronal devices (e.g., electrodes for deep brain stimulation,[7] retinal implants,[8,9] peripheral nerve stimulators,[10] and intracranial electrodes for diagnostic purposes[11]), further research is needed to design an ideal neuronal interface embracing a combination of electrical conductivity and flexibility/lightness, together with high biocompatibility. Graphene has attracted considerable attention due to its outstanding properties,[12–17] such as high electrical and thermal conductivity, mechanical strength, ultra-thinness, and biocompatibility, opening new

Dr. M. Moschetta, A. Podestà, O. Varvicchio, Prof. F. Benfenati, Dr. M. Bramini
Center for Synaptic Neuroscience and Technology
Istituto Italiano di Tecnologia
L.go Rosanna Benzi 10, Genova 16132, Italy
E-mail: mbramini@ugr.es

Dr. M. Moschetta, A. Podestà, O. Varvicchio
Department of Experimental Medicine
University of Genova
Viale Benedetto XV, Genova 16132, Italy

Dr. J.-Y. Lee, Dr. J. Son, Prof. G.-H. Lee
Department of Materials Science and Engineering
Seoul National University
Seoul 08826, Korea

Dr. J.-Y. Lee, Prof. G.-H. Lee
Research Institute of Advanced Materials (RIAM)
Seoul National University
Seoul 08826, Korea

The ORCID identification number(s) for the author(s) of this article can be found under https://doi.org/10.1002/adbi.202000177.

DOI: 10.1002/adbi.202000177

J. Rodrigues, Dr. A. Capasso
International Iberian Nanotechnology Laboratory
Braga 4715-330, Portugal
E-mail: andrea.capasso@inl.int

Dr. J. Son
Functional Composite Materials Research Center
Korea Institute of Science and Technology (KIST)
Jeollabuk-do 55324, Korea

Y. Lee, Prof. K. Kim
Department of Physics
Yonsei University
Seoul 03722, Korea

Y. Lee, Prof. K. Kim
Center for Nanomedicine
Institute for Basic Science (IBS)
Seoul 03722, Korea

Prof. G.-H. Lee
Institute of Engineering Research
Seoul National University
Seoul 08826, Korea

Prof. G.-H. Lee
Institute of Applied Physics
Seoul National University
Seoul 08826, Korea

perspectives in neuro-prosthetics.[18,19] Graphene has already been used as a flexible implant for in vitro and in vivo recordings,[20,21] field-effect transistors (FETs) for signal amplification of neural activity in vitro and in vivo,[22,23] superficial coating to foster neuronal growth and development,[24–26] and to target neuronal excitability.[27–31]

In an ideal neuron-friendly interface, high wettability and electrical conductivity are both required.[32,33] Pristine graphene presents high electrically conductivity but low wettability (i.e., showing a water contact angle >90° when supported on most substrates of interest),[34,35] and this can partially limit its biological applications. Several kinds of graphene-based materials (GBMs) with different morphologies and surface chemistry have been developed,[36] mainly by solution processing,[37] to maximize biocompatibility and improve the cell interfacing properties. Solution-processed graphene oxide (GO) flakes are an example of non-standard GBMs, whose wettability on the basal plane is generally higher than pristine graphene due to abundant (and uncontrolled in number) oxygen-containing groups. As a result, GO appeared to interact more easily with neurons in terms of membrane adhesion[30] and intracellular uptake,[27] but this also reflected in several unwanted effects connected with the morphology (edge-shaped) and size (sub-μm) of the GO flakes, and with a high internalization rate.[18,29] Besides, GO and its counterpart reduced-GO (rGO) have in general low electrical conductivity.[37] Chemical vapor deposited (CVD) graphene would be the ideal candidate to design a biological interface with high reproducibility and uniformity in properties over large areas.[38–41] To comply with the aforementioned neuron interfacing requirements, surface strategies aimed at turning CVD graphene to hydrophilic without sacrificing other crucial characteristics for in vitro and in vivo tissue engineering applications can play a pivotal role.[42,43] Recently, it was reported that the wettability of graphene could be controlled by hydrogenation and fluorination, which represent valuable alternatives to more invasive surface modifications.[44–46] Also, we reported that hydrogenated graphene (HGr) was utilized as well-developed biocompatible platform for selective cell culturing. Moreover, Son and colleagues[46] recently tested HGr with living cells (GFP-MCF-7 human breast cancer cell line). Their results showed that the cell density, and thereby the adhesion, was considerably higher on the hydrophilic HGr substrate than on the hydrophobic pristine graphene. This behavior indicated a high biocompatibility of the HGr substrate.

Previous studies demonstrated that graphene can be a suitable interface for biological applications when supported on rigid and stiff substrates, such as glass.[24,25,47–50] The search for more versatile substrates is actively pursued and poly(ethylene terephthalate) (PET) appears as a very appealing candidate for biomedical implants, thanks to the combination of transparency, flexibility and biocompatibility: For these reasons, it has been used as a substrate to fabricate graphene-based electrodes for in vitro and in vivo neuronal stimulation and recording.[51–54] In the present work, we developed a graphene-based biological interface for primary neuronal networks. Pristine CVD graphene was hydrogenated by a remote and non-destructive hydrogen plasma approach. As fabricated hydrophilic HGr was transferred onto flexible and lightweight PET substrates, forming a bio-compatible interface with high wettability, crucial for the neuronal interface, while retaining electrical conductivity. In our study, primary neurons grown onto PET/HGr displayed high cellular adhesion and preserved physiological intrinsic firing properties. Remarkably, the mature neuronal networks formed on PET/HGr exhibited an improved neuronal signaling, demonstrated by a two-time higher miniature post-synaptic excitatory frequency with respect to PET/Gr. PET/HGr exhibited an enhanced excitatory transmission, which is two times higher than PET/Gr. On the contrary, neuronal networks on PET/Gr presented an overall altered morphology due to an intrinsic low wettability. We demonstrate that wettability rather than conductivity is of the utmost importance for the formation of mature neuronal network, although a suitable balance between the two properties, like in the case of PET/HGr, is key to enhance neuronal excitability. Our work shows a solid alternative approach and moves a step forward toward flexible implants by fabricating PET/HGr neuronal interfaces. Overall, conferring a superficial electrical conductivity to a versatile biocompatible substrate (i.e., PET) could further enable its use in neuroscience.

2. Results and Discussion

Graphene was grown by CVD and transferred on PET substrates (2.5×2.5 cm^2) as shown in **Figure 1**a. PET is one of the most common polymers used in the industry because of its strength, lightweight, formability, thermal, and chemical stability.[55,56] PET, biocompatible and fluorescein diacetate (FDA)-approved, has been widely used in biomedical applications (e.g., tissue engineering for soft tissue repair[57]) for its flexibility and transparency. For these reasons, PET was chosen as substrate of interest for this study. Hydrogenated graphene (HGr) was prepared by processing graphene with indirect hydrogen plasma (See Experimental Section for details). Because of possible degradation of the PET substrates by acetone in the conventional graphene transfer process with poly(methyl methacrylate) (PMMA), ethyl cellulose (EC) was used as a supporting film and removed by ethanol.[58] EC, a bio-compatible material commonly used as a coating for medicinal pills and drug delivery systems,[59,60] left less residue than PMMA after the transfer,[61] making such EC transfer approach specifically suited to graphene bio-applications. Graphene transferred on PET substrate was characterized by Raman spectroscopy. Figure 1b shows the Raman spectra of bare PET, PET/Gr, and PET/HGr after a 3-hour hydrogenation. Two main characteristic peaks of monolayer graphene, the G peak at ≈1580 cm^{-1} and the 2D peak at ≈2700 cm^{-1}, are clearly visible in the spectra of both PET/Gr and PET/HGr. The other peaks correspond to the background signals originating from

Prof. F. Benfenati
IRCSS Ospedale Policlinico San Martino
L.go Rosanna Benzi 10, Genova 16132, Italy
Dr. M. Bramini
Department of Applied Physics
Faculty of Science
University of Granada
Granada 18071, Spain

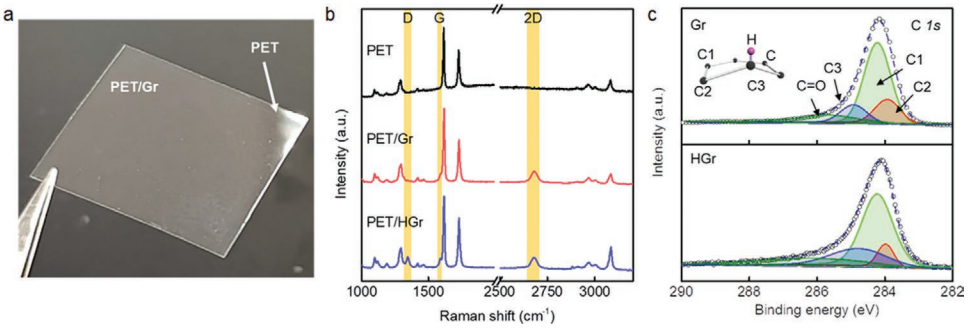

Figure 1. Structural and chemical characteristics of Gr and HGr. a) Optical image of the transferred graphene film on PET substrate. The graphene film is not clearly visible on PET due to the high transparency. b) Raman spectra of PET, PET/Gr, and PET/HGr samples. The peaks indicated with D, G, and 2D (yellow regions) are from Gr and HGr. Other peaks are from PET substrate. c) C 1s core-level XPS spectra of Gr and HGr. The sp^3-type bonds increased after hydrogenation of Gr.

the PET substrate.[62] The absence of the D peak in Gr/PET indicates that the synthesized graphene has high quality and no defects are generated during the transfer process. Meanwhile, the presence of the D peak in PET/HGr indicates the formation of C—H sp^3 bonds, as previously reported.[44] To verify the formation of C—H bonds by hydrogenation, the chemical state and elemental composition of Gr and HGr were probed by X-ray photoelectron spectroscopy (XPS). Figure 1c shows the C 1s core-level spectra of the two samples transferred on a SiO_2/Si substrate. The C1s spectra of Gr and HGr can be fitted with four components (C1, C2, C3, and C=O). The main peak at ≈284.5 eV (C1) is attributed to graphitic C=C sp^2 carbon. The C2 and C3 peaks result from sp^2 carbon adjacent to a C—H bond (C*—C) and sp^3 carbon coordinated with a hydrogen atom (C—H), respectively. After hydrogenation, the C1 carbon peak decreased, while the C3 peak increased, indicating that graphene was hydrogenated by the formation of sp^3 C—H bonds.[44] We compared the hydrogen content in Gr and HGr by evaluating the areas of the C1, C2, and C3 peaks, and found that the amount of hydrogen increased from 12 to 23% after the hydrogenation process.[63]

We further confirmed the non-destructive effect of the hydrogen plasma treatment used in this work, by analyzing the samples with scanning transmission electron microscopy (Figure S1, Supporting Information). We additionally measured electrical resistivity and water contact angles (WCA) of Gr and HGr, as both properties strongly influence the substrate interactions and functional behavior of neuronal cells.[24,64] Graphene FETs were fabricated on SiO_2 (285 nm)/Si substrates as shown in the inset of **Figure 2**a. As shown in the resistivity versus gate voltage curves of the Gr and HGr devices (Figure 2a), the charge neutrality point of Gr before hydrogenation was ≈60 V, in agreement with the fact that the as-grown Gr is generally p-doped due to polymer residue, adsorbed and trapped molecules and charged impurities from the SiO_2 substrate, as previously reported.[65] The sheet resistances (R_s) of Gr and HGr were measured by using transmission line method (TLM) at zero gate voltage. After hydrogenation of graphene for 3 h, the sheet resistance of HGr (3300 Ω □$^{-1}$) became higher than that of the as-grown Gr (563 Ω □$^{-1}$). Differently from fully HGr (almost insulating), our HGr still retains a moderate conductivity, possibly due to an increased p-doping.[44] The Raman

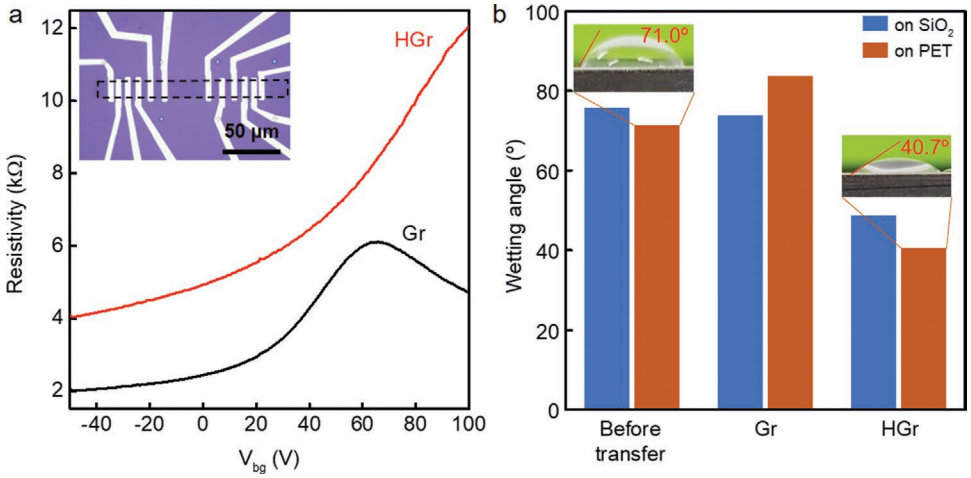

Figure 2. Electrical resistivity and wettability of Gr and HGr. a) Resistivity of Gr and HGr FETs as a function of back gate voltage (V_{bg}). The inset shows an optical image of the graphene-based FET with TLM geometry. b) Water contact angle of Gr and HGr on Si/SiO_2 (blue) and PET (brown) substrates, before and after hydrogenation. As-transferred Gr is rather hydrophobic, while HGr becomes hydrophilic. The inset images show photos of water droplets used in the measurements.

spectrum shown in Figure 1b along with the moderate conductivity seem to indicate that our HGr is partially hydrogenated. We calculated the field-effect mobility (μ_{FE}) of Gr and HGr by using the Equation (1) below:

$$\mu_{FE} = \frac{L}{WC_i V_{ds}} \left(\frac{dI_{ds}}{dV_{bg}} \right) \quad (1)$$

where L, W, and C_i are channel length, width, and capacitance, respectively. The field-effect mobility of HGr (200 $cm^2\ Vs^{-1}$) was lower than that of Gr (1144 $cm^2\ Vs^{-1}$) due to defect scattering by sp^3 C—H bonds. Wettability of graphene is another important factor to determine the activity of neurons plated on the graphene. Thus, we measured the WCA of water droplets (30 µL) on Gr and HGr samples supported on either Si/SiO_2 or PET substrates, since it has been proposed that the wetting angle of graphene can be affected by the substrate (showing so-called wetting transparency[34]). As shown in Figure 2b, the bare SiO_2/Si and PET substrates showed WCA of 74.8 and 71.0°, respectively.[66,67]

Upon transfer of CVD graphene films onto the substrates, the WCA increased to 73.7 and 83.7° on SiO_2 and PET, respectively. In spite of the small differences in wettability of the transferred graphene samples, the graphene surface remains rather hydrophobic, regardless of the substrate. However, after hydrogenation, the WCA of HGr dramatically decreased to 48.4 and 40.7° on SiO_2 and PET, respectively, consistent with previous results indicating that the sp^3 bonds in the HGr lead to a strong interaction between graphene and water.[64,68] Thus, the possibility exists that the electrical conductivity and chemical functional groups of HGr are beneficial for enhancing the interactions with neurons due to charge transfer and enhanced adhesion.[69]

Survival and adhesion of rat primary cortical neurons grown onto the two kinds of graphene supports were investigated after 14 days. As shown in **Figure 3**, neurons plated onto PET, glass, PET/Gr, and PET/HGr were live-stained with fluorophores for determining the extent of cell death and survival by fluorescence microscopy (Figure 3a and Figure S3a, Supporting Information) and the results were normalized to the glass substrate, the standard condition for in vitro neuronal culture. The results of Figure 3b clearly suggest that both viability and adhesion of neurons were impaired on PET substrates, while no effect was observed onto PET/Gr and PET/HGr supports. Notably, the morphology of the developed network on PET/Gr was slightly different as compared to glass and PET/HGr substrates. In particular, scanning electron microscopy (SEM) and confocal laser scanning microscopy confirmed the presence of cell clusters and aggregates of neurons only on PET/Gr supports that were not present under the other culturing conditions (Figure 3a and Figure S3b, Supporting Information), likely due to the hydrophobicity of Gr.

However, neurons grown on PET/HGr showed a network morphology with homogenous distribution of cells, similar to that observed on standard glass substrates. Being neurons viable on all graphene substrates, it was crucial to understand whether the surface characteristics were affecting their physiological activity. To this end, single patch-clamp recordings were performed. While on PET only few cells could be patched, and showed abnormal passive membrane properties, cortical neurons placed onto glass, PET/Gr, and PET/HGr displayed comparable passive membrane properties and intrinsic excitability (Figure 3c,d and Table S2, Supporting Information). Usually, carbon-based materials exhibit high electrical conductivity, leading researchers to think that graphene could improve neuronal activity and communication. Indeed, numerous studies showed how neurons grown on GBMs present an improved cell excitability, essentially due to changes in ion channel expression (in particular K^+ and Na^+ channels).[24,70,71] Interestingly, our data suggest that graphene is not able to induce per se modification of the channel composition and cell excitability, regardless of the level of conductivity of the substrate, being it either PET/Gr or PET/HGr. What instead seems to be the crucial parameter, in addition to electrical conductivity, for the creation of an efficient neuronal interface is the surface wettability, which allows neurons to correctly adhere onto the conductive substrate and develop a morphologically mature and highly structured network. This is in line with recent studies showing that GO is more efficient in promoting adipose-derived stem cells as compared to rGO, in spite of a reduced electrical conductivity.[72]

Since Gr and HGr have no differential influence on survival and intrinsic electrophysiological properties of single neurons, we investigated their effects on the physiological network properties, recording both excitatory (*E*) and inhibitory (*I*) miniature postsynaptic currents (mPSCs) (**Figures 4** and **5**, Figures S4 and S5, Supporting Information). Although no differences were noticed in mIPSCs (Figures S4 and S5, Supporting Information), the recording of mEPSCs showed instead interesting results. We measured excitatory synaptic transmission by recording mEPSCs in the presence of the sodium-channel blocker tetrodotoxin (TTX, 300 nM) (Figure 4a). According with the quantal properties of synaptic transmission, the amplitude of miniature events (quantal content) reflects the neurotransmitter content of synaptic vesicles (SVs) and the postsynaptic effect of the neurotransmitter, while the frequency is dependent on the density of active synapses and the stochastic fusion properties of single SVs.[73] Primary neurons on PET/HGr showed an enhanced mEPSC frequency in the absence of significant changes in the amplitude, which has been confirmed by the cumulative distribution of the inter-event intervals and amplitude (Figure 4b,c). The enhanced frequency of mEPSCs and the resulting excitation/inhibition imbalance in neurons grown onto PET/HGr (Figures 4 and 5; Figures S4 and S5, Supporting Information) suggest the presence of a potential increase in the network firing activity. To address this point, we recorded the spontaneous firing of action potentials under basal conditions, without altering synaptic transmission (Figure 4d). In accordance with the electrophysiological results, we observed that neurons plated onto PET/HGr showed a significant increase in firing rate, as compared to the other experimental conditions considered (Figure 4e).

By evaluating the release dynamics of single miniature events, we observed an increase in the mEPSC rise time in neurons grown onto PET/Gr and PET/HGr, leading to an increase of the overall synaptic charge (Figure 5). Taken together, these results can be ascribed either to an enhanced neuronal

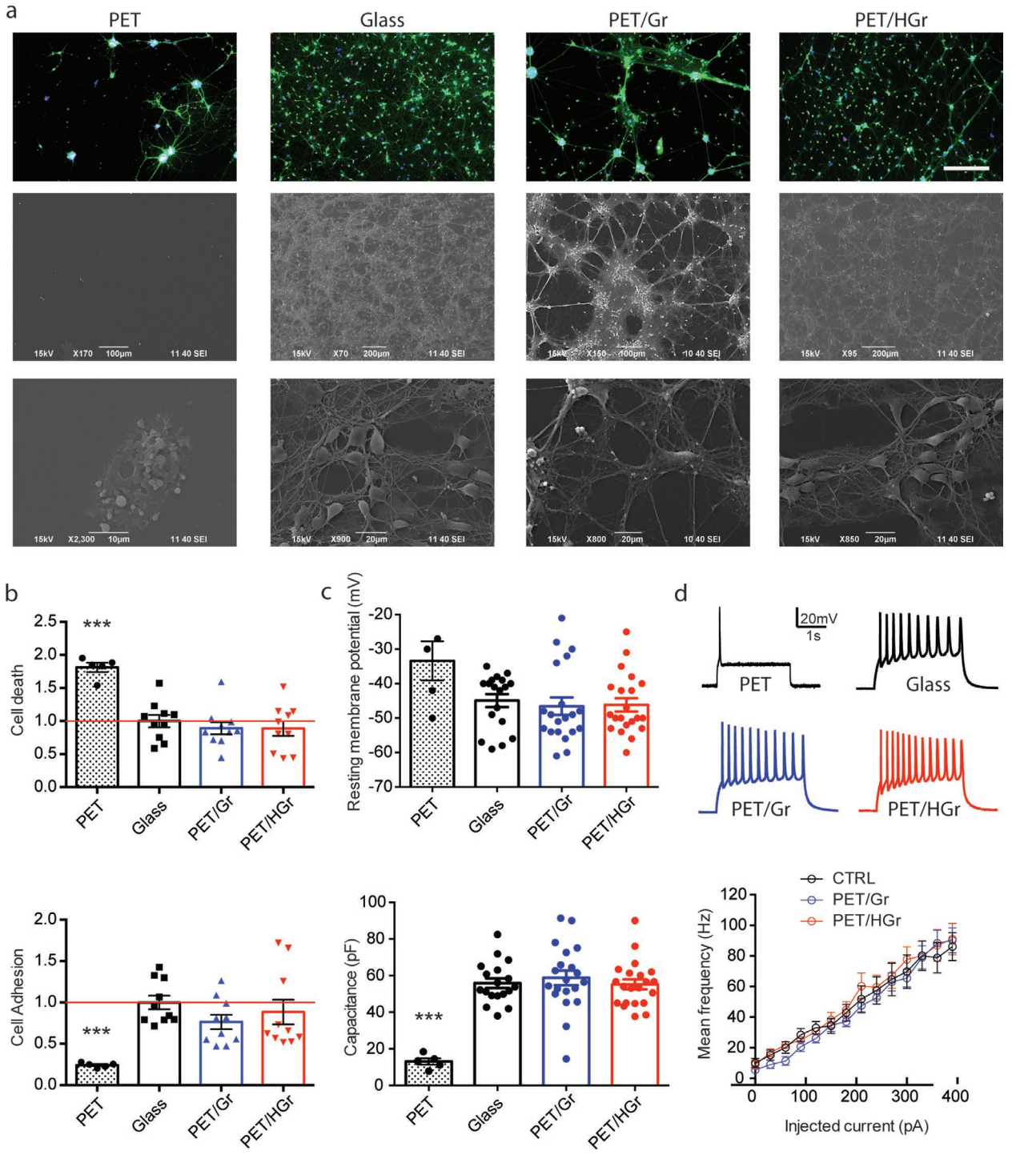

Figure 3. Adhesion, viability, and firing properties of neurons on graphene substrates. a) Primary rat cortical neurons were grown onto PET, glass, PET/Gr, and PET/HGr for 14 days. Cell adhesion and viability were evaluated by fluorescence microscopy. Upper panel: Representative images of neuronal cultures stained with Hoechst 33342 (blue) for nuclei visualization, fluorescein diacetate (FDA, in green) for cell viability and propidium iodide (PI, in red) for cell death (scale bars: 100 μm). Middle and lower panels: SEM micrographs of cultured neuronal networks. Except for PET samples, where very few cell bodies were found, cell morphology was substantially unaffected, although the neuronal networks on PET/Gr display cell aggregation and clamping. b) The percentages of PI-positive cells with respect to the total number of Hoechst-positive cells, calculated for each experimental group, were normalized to the values of untreated samples (glass substrate) set to 1. Except for bare PET, no significant changes in cell death were observed under all the experimental conditions (one-way ANOVA/Bonferroni's tests, 2000 cells from $n = 10$ fields per experimental condition, from two independent neuronal preparations). c) Electrophysiological recordings of membrane resting potential (upper panel) and membrane capacitance (lower panel) performed by whole cell patch-clamp. d) Upper panel: Representative firing traces in response to current injection. Lower panel: The mean ± SEM firing frequency with respect to the injected current is also shown (right). No significant differences were found among samples (one-way ANOVA/Bonferroni's tests, $n = 20$ cells per experimental condition, from three independent neuronal preparations).

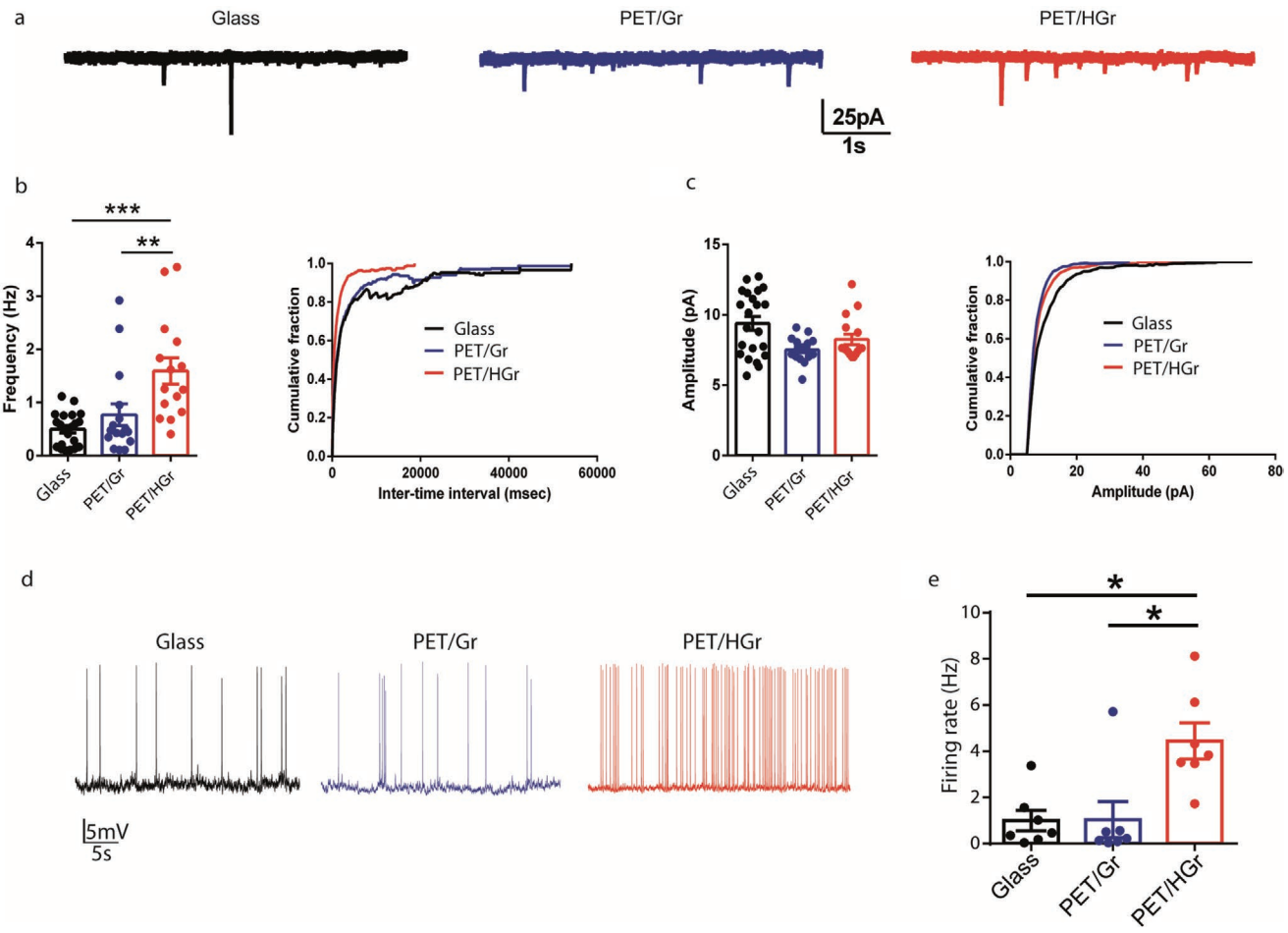

Figure 4. HGr enhances mEPSC frequency and spontaneous action potentials in rat cortical neurons. a) Representative traces of mEPSCs recorded at –70 mV in 13–15 DIV rat cortical neurons plated on glass (black), PET/Gr (blue) and PET/HGr (red). b) Histograms showing the average mEPSC frequency (left) and the respective cumulative plot of inter-event intervals (right). c) Histograms showing the average mEPSC amplitude (left) and the respective cumulative plot of amplitude (right). All data are means ± SEM; $n = 22$, 15, and 16 neurons, respectively, taken from three independent preparations. ** $p < 0.01$ and *** $p < 0.001$; ANOVA/Bonferroni's tests. d) Representative traces of action potentials recorded at resting membrane potential in 13–15 DIV rat cortical neurons plated on glass (black), PET/Gr (blue), and PET/HGr (red). e) Histograms showing the substrate-dependent changes in the spontaneous firing rate. All data are means ± SEM; $n = 7$ neurons for all the three conditions. *$p < 0.05$; ANOVA/Bonferroni's tests.

maturation associated with an increased density of excitatory synaptic contacts or to an altered release probability.[73]

To sort out these possibilities, we double-stained the networks with the presynaptic marker vesicular glutamate transporter (VGLUT) and the neuronal marker β-III tubulin. An increased number of excitatory synaptic puncta was observed selectively in networks grown onto PET/HGr, paralleling the enhanced mEPSC frequency and excluding a marked change in SV release probability (**Figure 6**). The increased mEPSC charge and dynamics observed in neurons plated on both PET/Gr and PET/HGr suggest that additional effects due to Gr-interaction are present either post-synaptically or in probability of spontaneous release at the presynaptic level.[25] Except for the modest change in mEPSC dynamics, neurons plated on PET/Gr displayed an electrophysiological behavior comparable with those plated on glass as previously similarly described.[24] The high wettability generated by the hydrogenation process is likely at the basis of the enhancement of network maturation and active synapse formation of neurons.[32] Similarly, this hypothesis holds also for the improved interactions between neurons and astrocytes with pristine Gr, GO, and rGO.[27,28,74]

We finally analyzed the PET-supported samples used in our assay to evaluate the effect of the neurons on the underlying graphene materials. Figure S6, Supporting Information, shows the Raman spectra taken on PET/Gr and PET/HGr samples, as detailed in the Experimental Section. The spectral features are discussed in the Supplementary Information.

The G and 2D peak position is analyzed in **Figure 7**, to discriminate between the effect of mechanical strain and charge doping on the graphene-based substrates before and after the interaction with the neurons.[75] In the case of Gr, $P_{Gr}(\omega_G,\omega_{2D})$ moves along the "strain-free" direction, evidencing a decrease in the initial p-doping state of the pristine Gr in presence of neurons (Gr→Gr+N), and a partial restoration of the initial p-doping state upon neuron removal (Gr+N→Gr-N). In the case of HGr

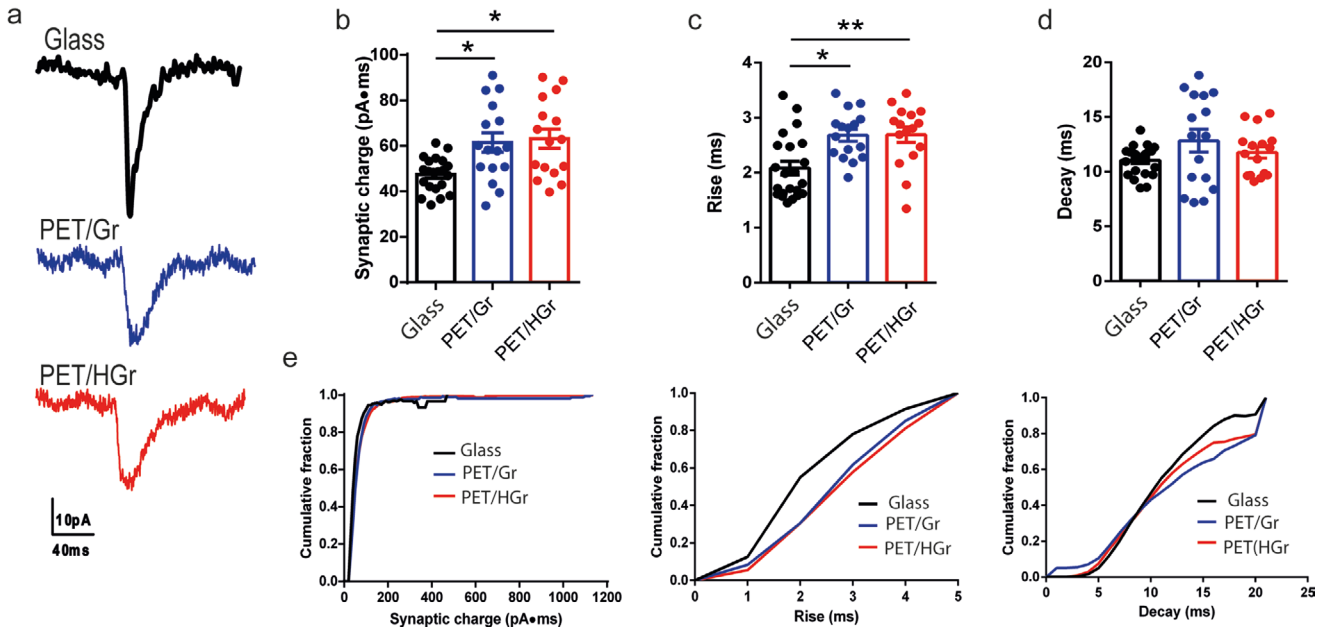

Figure 5. PET/HGr and PET/Gr alter mEPSC kinetics in rat cortical neurons. a) Representative traces of individual mEPSC events over an enlarged timescale. b–d) Histograms showing b) synaptic charge, c) rise times, and d) decay times. e) From left to right: Corresponding cumulative plots of synaptic charge, rise time, and decay times, respectively. Data in panels (b–d) are means ± SEM; n = 22, 15, and 16 neurons, respectively, from three independent preparations. *$p < 0.05$ and **$p < 0.01$; ANOVA/Bonferroni's tests.

the situation is different, since $P_{HGr}(\omega_G,\omega_{2D})$ in presence of neurons moves primarily along the "charge-neutral" direction, demonstrating the occurrence of tensile strain (HGr→HGr+N). When neurons are removed, $P_{HGr}(\omega_G,\omega_{2D})$ does not move back along the same direction, but it rather moves along the p-doping vector (HGr+N→HGr-N), partly recovering its initial level of p-type doping. This analysis suggests that neurons seem to not firmly adhere on Gr (due to its low wettability) and, as a result, to possibly slide on the surface during the network formation (causing no strain-related effects on Gr). However, having Gr a high electrical conductivity, an efficient electrical interaction with neurons can take place (due to an electron transfer from the neurons), with an overall effect of p-doping recovery upon neuron removal. In the case of HGr, the situation is crucially different: neurons could be expected to adhere more strongly to HGr thanks to high wettability so that, when a mature and functional network is formed, a tensile strain may be induced in the underlying HGr film. Other than having high wettability, HGr might as well be semi-suspended from the substrate as an effect of strong adhesive forces exerted by the neurons (as similarly occurs when graphene interacts with alkane layers[76]) or even be corrugated (as C—H bonds can weaken the interaction with the substrate[77]): These two conditions could further motivate a strong mechanical interaction between neurons and HGr, and should be investigated more in the future.

3. Conclusions

The use of graphene in neuroscience is still in a nascent stage, with numerous challenges to be yet overcome. Our study shows that a controlled modification of graphene by hydrogenation can be used to tailor its surface properties and promote neuronal adhesion and network maturation, while simultaneously modulating neuronal activity. Because of its wettability and residual conductivity, HGr promotes excitatory synaptic transmission and connectivity in primary neuronal networks. The development of highly biocompatible and conductive graphene-based templates on transparent and flexible substrates, such as PET, is highly significant in the framework of neurodegenerative diseases, where neurons need to be targeted with high specificity to preserve the physiological activity of the system. Importantly, we suggest that wettability more than conductivity is a key parameter for building efficient neuronal interfaces. In this respect, the HGr developed in this study is more suited as bio-interface than the various forms of functionalized graphene[44] because of its tunable wettability and high biocompatibility, as well as negligible chemical contamination. Concerning the mechanism of the interaction between neurons and our GBMs, the post-hoc Raman analysis indicates that Gr only vary its doping state through an electrostatic interaction with the neurons, while HGr could undergo a strain change possibly due to a stronger physical interaction with the neuronal network. Being such modification stable over long times, it is tempting to imagine a future in vivo application of this graphene-based material in prosthetic devices. Interestingly, the remote plasma hydrogenation process used in this paper can be aptly tuned to vary the hydrogenation level of graphene (and thus the consequent wettability to conductivity ratio), and can be also patterned with a simple hard mask. Overall, HGr on PET and other polymeric substrates constitute a class of neuronal interfaces to be further explored and exploited in biological environments.

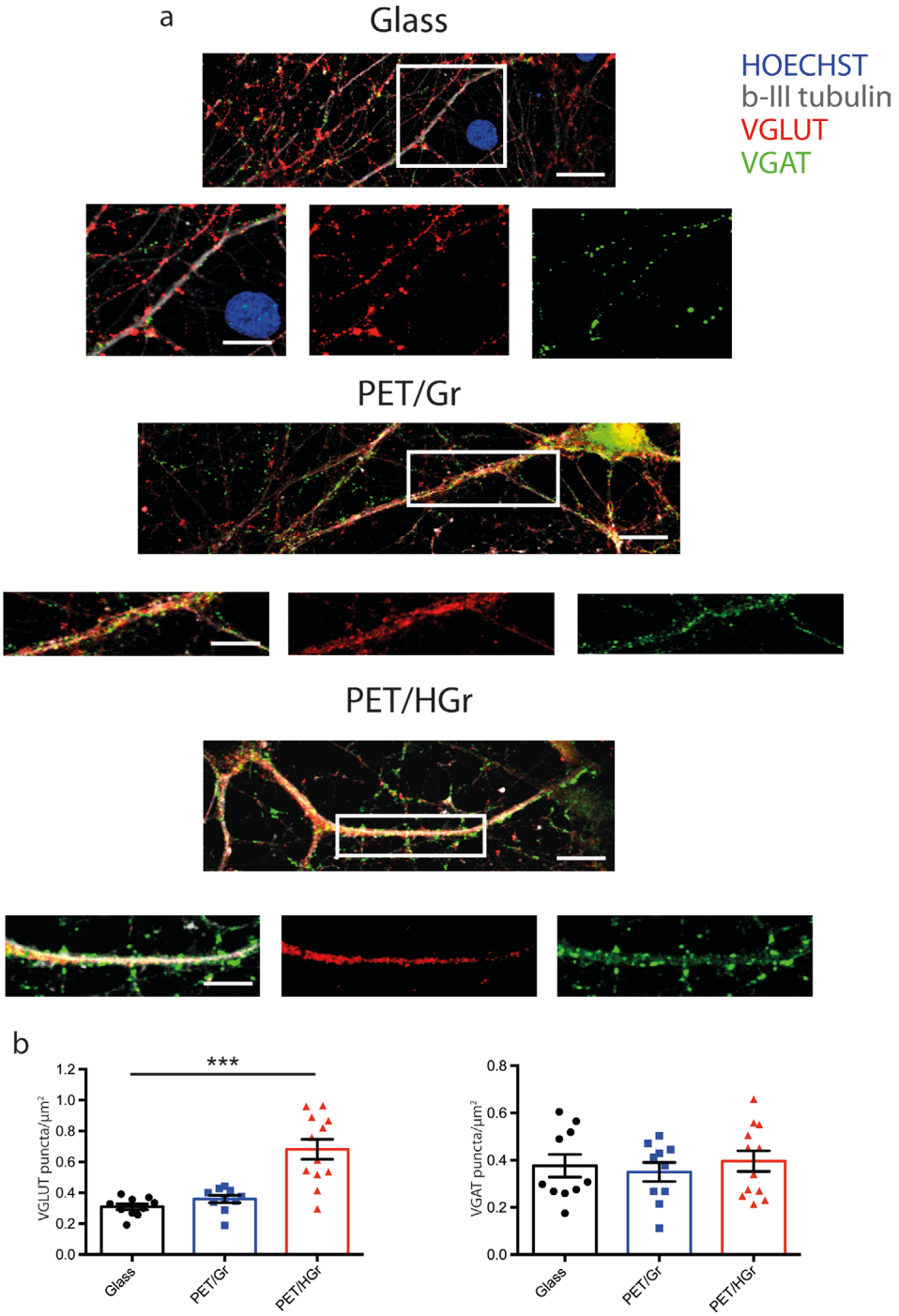

Figure 6. Density of excitatory and inhibitory synapses in neuronal networks grown onto PET/HGr and PET/Gr surfaces. a) Representative images of neurons stained for ßIII tubulin (gray), VGLUT (red), and VGAT (green). Nuclei were stained with Hoechst 33 342 (blue). Scale bars: 10 µm in the main images and 5 µm in zoomed images (glass); 5 µm in the main image and 3 µm in zoomed images (PET/Gr and PET/HGr). b) Density of VGLUT-positive excitatory synapses (left) and VGAT-positive inhibitory synapses (right) in neurons grown for 14 days in vitro onto Glass, PET/Gr, and PET/HGr supports. Data are expressed as means ± SEM. ***p <0.001, one-way ANOVA/Bonferroni's tests (n = 10–12 cells per experimental condition from two independent culture preparations).

4. Experimental Section

Growth of Monolayer Graphene by CVD on Cu Foil: Graphene was synthesized on a 25-µm-thick copper foil (Alfa-Aesar, 99.8%) using a low-pressure chemical vapor deposition in a quartz-tube furnace (SciEnTech, TCVD50). A copper (Cu) foil was cut into 2 cm× 10 cm substrates and put on an alumina boat, which was loaded into the quartz tube. After loading the substrate, sequential purging and venting was performed

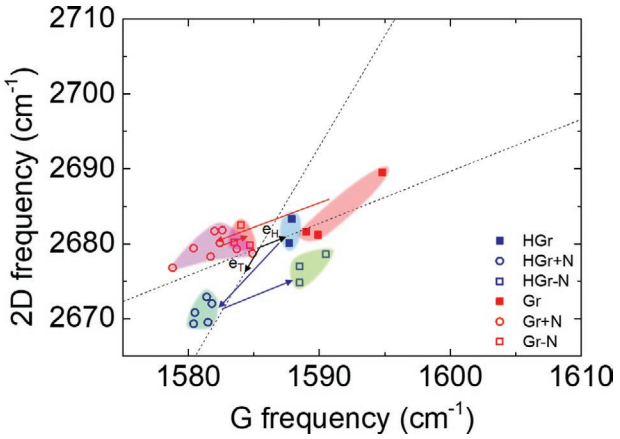

Figure 7. Raman analysis of mechanical strain versus charge doping on the graphene-based substrates in biological conditions. Raman spectra are collected and analyzed for PET/Gr and PET/HGr in three different settings: 1) in pristine conditions (Pristine), 2) with grown neurons (+ Neurons), 3) and after the neurons were removed from the substrate (– Neurons). Each point represent the position of the G and 2D peaks for the respective samples, indicated in the text as $P_{sample}(\omega_G,\omega_{2D})$.[75] The two dashed line represent expected (ω_G,ω_{2D}) variations for graphene undergoing two different kinds of changes: i) "strain-free" condition with varying density of holes (indicated by the e_H unit vector, toward increasing p-doping) and ii) "charge-neutral" condition under uniaxial stress (indicated by the e_T unit vector, toward increasing tensile stress).[75]

with Ar. After that, the temperature was ramped to 1000 °C in 10 min while flowing 15 sccm of H_2, and then kept at 1000 °C for 1 h with the same gas flow to anneal the Cu substrate. Graphene was grown by flowing H_2 (15 sccm) and CH_4 (35 sccm) for 30 min. After completion of growth, the sample was removed from the furnace center to cool down quickly, maintaining the gas flow rate of H_2 and CH_4. The whole process was operated under vacuum condition.

Transfer of Monolayer Graphene on Substrates: The as-grown CVD graphene was transferred on target substrate, Si/SiO_2 (285 nm oxide), or PET (GoodFellow, ES30125). To prevent damaging PET film under acetone, EC was utilized as supporting film instead of PMMA[43]. First, graphene/Cu foil was-spin coated by EC (2 wt% in ethanol) at 2000 rpm for 90 s, followed by removing uncoated graphene using oxygen plasma (100 kHz, 100 W, 20 sccm O_2, 2 min). Before etching Cu foil under EC/graphene film, cut samples using razor blade to required size. The prepared EC/graphene/Cu samples was floated on etching solution (Copper etchant, Sigma-Aldrich) for 4–5 h, and rinsing residual etchant under graphene layer after Cu etching by floating samples on clean water bath repeatedly. Then, EC/Graphene sample was scooped using PET substrate gently and store under vacuum to remove trapped water between PET and graphene, and place inside a 100 °C oven for 10 min to improve adhesion. Finally, put EC/Graphene/PET sample into warm ethanol bath (50 °C, 2 min) to remove EC layer and dried using nitrogen gun.

Plasma Treatment on Graphene/PET: The low-frequency indirect plasma system (50 kHz, 20 W, 20 sccm of H_2) was utilized for hydrogenation of graphene. Graphene/PET sample, located 3 cm away from plasma generation zone, was treated for 3 h to prevent severe damage.

Characterization of Graphene: Raman measurements were conducted in the Raman spectroscopy (Renishaw, inVia) by using a 532 nm-wavelength laser. Water contact angle measurements were performed under ambient condition. A water droplet of 30 µL was deposited on a graphene/PET or graphene/SiO_2 by micropipette and contact angle was measured by photo. For XPS measurements we used a Kratos Axis Ultra X-ray photoelectron spectrometer (Kratos Analytical, Inc., Manchester, UK) using monochromatic Al Kα radiation (1486.6 eV). High-resolution spectra were collected at a take-off angle of 90° using pass energy of 40 eV from a 0.7 mm × 0.3 mm area using the hybrid (electrostatic and magnetic immersion) lens mode. The samples were affixed onto the sample holder using double-sided office tape. The binding energy scale of the instrument was calibrated using the Cu 2p (932.7 eV) and Au 4f (84.0 eV) photoelectron lines. The binding energies were referenced to the graphitic C 1s signal at 284.5 eV. The pressure during analysis was 7×10^{-7} Pa.

Device Fabrication and Measurement: CVD graphene transferred on Si/SiO_2 substrate were patterned by e-beam lithography and etched by oxygen plasma to fabricate the graphene channels. Metal electrodes were patterned by e-beam lithography and Cr/Pd/Au (1 / 30 / 40 nm) metals were deposited by an e-beam evaporator. Electrical properties were measured by a semiconductor parameter analyser (SCS-4200, Keithley) under ambient condition.

Transmission Electron Microscopy: CVD-grown graphene was transferred on holey carbon film deposited TEM grid (Quantifoil) by a direct transfer method.[78] TEM grid was placed on graphene/Cu, and a droplet of isopropanol was dropped on the surface of TEM grid. After evaporation of IPA naturally, the sample was floated on copper etchant (0.1 M ammonium persulfate solution) for 2–3 h. The copper etched graphene/TEM grid was sequentially moved to deionized water to remove residual chemical several times and dried naturally. TEM imaging were performed by a JEOL JEM-ARM200F equipped with image and probe aberration correctors operated at 80 kV.

Preparation of Primary Neurons: All experiments were carried out in accordance with the guidelines established by the European Community Council (Directive 2010/63/EU of 22 September 2010) and were approved by the Italian Ministry of Health. Primary cortical cultures were prepared from wild-type Sprague-Dawley rats (Charles River, Calco, Italy). All efforts were made to minimize suffering and to reduce the number of animals used. Rats were sacrificed by CO_2 inhalation, and 18-day embryos (E18) were removed immediately by cesarean section. Briefly, enzymatically dissociated cortical neurons were plated on poly-D-lysine-coated (0.1 mg mL^{-1}) PET, glass coverslips (Thermo-Fischer Scientific, Waltham, MA), PET-Gr and PET-HGr supports at a density of 100 000 cells mL^{-1}. Cultures were incubated at 37 °C, 5% CO_2, 90% humidity in medium consisting of Neurobasal (Gibco/Thermo-Fischer Scientific) supplemented to reach final concentration of 5% L-glutamine (200 mM), 5% penicillin (10 000 units mL^{-1}) / streptomycin (10 000 µg mL^{-1}) and 10% B27 supplement (Gibco/Thermo-Fischer Scientific). All chemicals were purchased from Life Technologies/Thermo-Fischer Scientific unless stated otherwise.

Preparation of Graphene Substrates for Post-Experiment Raman Analysis: To perform the post-experiment Raman spectroscopy, graphene substrates were prepared and cortical neurons were seeded onto glass coverslips, PET/Gr and PET/HGr substrates as previously described. After 14 days, Neurobasal complete medium was removed from each sample and neurons were washed with phosphate-buffered saline (PBS). Half of the samples were enzymatically treated to completely remove neurons from the substrates, washed with ethanol (70%) and let dry under the hood. The remaining half of the samples were directly let dry under the hood without removing neurons.

Cell Viability and Density: Rat cortical neurons were seeded onto PET, glass coverslips, PET/Gr, and PET/HGr supports for 14 days. Live cells were stained with propidium iodide (PI; 1 µM) for cell death quantification, FDA (2 µM) for cell viability, and Hoechst 33 342 (1 µM) for nuclei visualization for 3 min at room temperature (RT). Cell viability was quantified at 20× (0.5 NA) magnification using a Nikon Eclipse-80i upright epifluorescence microscope (Nikon, Tokyo, Japan), with random sampling of ten fields per sample ($n = 2$ samples, from two independent culture preparations). The values are obtained by ratio of PI/Hoechst 33 342 positive cells and normalized for the Ctrl (Glass) samples. Cell density was calculated by counting the total number of Hoechst 33 342 positive cells. Image analysis was performed using the ImageJ software and the Cell Counter plugin.

Immunocytochemistry and SEM: Rat cortical neurons were fixed in PBS/4% paraformaldehyde for 20 min at RT. Cells were permeabilized with 1% Triton ×-100 for 5 min, blocked with 2% fetal bovine serum in PBS/Tween 800.05% for 30 min at RT, and incubated with primary antibodies in the same buffer for 45 min. The primary antibodies used were: rabbit polyclonal anti-β-tubulin III (#T2200, Sigma-Aldrich), mouse monoclonal anti-glial fibrillary acidic protein (GFAP, #G3893, Sigma-Aldrich), guinea pig polyclonal anti-vesicular glutamate transporter-1 (VGLUT1, #AB5905, Millipore), and rabbit polyclonal anti-vesicular GABA transporter (VGAT, #131003, Synaptic System). After the primary incubation and several PBS washes, neurons were incubated for 45 min with the secondary antibodies in blocking buffer solution. Fluorescently conjugated secondary antibodies were from Molecular Probes (Thermo-Fisher Scientific; Alexa Fluor 488 #A11029, Alexa Fluor 568 #A11036, Alexa Fluor 647 #A21450). Samples were mounted in ProLong Gold antifade reagent with DAPI (#P36935, Thermo-Fisher Scientific) on 1.5-mm-thick coverslips. Image acquisitions were performed using a confocal microscope (SP8, Leica Microsystems GmbH, Wetzlar, Germany) at 40× (1.4 NA) magnification. Offline analysis was performed using the ImageJ software and the Threshold tool to convert signals into a binary system. For each set of experiments, all images were acquired using identical exposure settings; VGAT and VGLUT values were identified as puncta after binary transformation. Their number was normalized to the respective neurite area calculated on the basis of βIII-tubulin labeling. For SEM cell analysis, primary cortical neurons after 14 days were fixed with 1.5% glutaraldehyde in 66 mM sodium cacodylate buffer and post-fixed in 1% OsO_4. Sample dehydration was performed by 5 min washes in 30%, 50%, 70%, 80%, 90%, 96%, and 100% EtOH solutions. In order to fully dry the samples, specimens were left in 100% EtOH overnight until complete evaporation. Before SEM acquisition, coverslips were sputter-coated with a 10 nm layer of 99% gold nanoparticles in an Ar-filled chamber (Cressington, Sputter Coater 208HR) and imaged using a JEOL JSM-6490LA scanning electron microscope (JEOL Ltd., Tokyo, Japan).

Patch-Clamp Recordings: Rat cortical neurons were recorded at 12–15 DIV. Patch pipettes, prepared from thin borosilicate glass, were pulled and fire-polished to a final resistance of 4–5 MΩ when filled with standard internal solution. All experiments were performed at RT (22–24 °C). Data acquisition was performed using PatchMaster program (HEKA Elektronic). Current-clamp recordings were performed at a holding potential of –70 mV, and action potential firing was induced by injecting current steps of 10 pA lasting 500 ms. Cells were maintained in extracellular standard solution (Tyrode) containing (in mM): 140 NaCl, 2 $CaCl_2$, 1 $MgCl_2$, 4 KCl, 10 glucose, and 10 HEPES (pH 7.3 with NaOH), in which D-(–)-2-amino-5-phosphonopentanoic acid (D-AP5; 50 μM), 6-cyano-7 nitroquinoxaline-2,3-dione (CNQX; 10 μM), bicuculline methiodide (BIC; 30 μM), and (2S)-3-[[(1S)-1-(3,4-dichlorophenyl)ethyl] amino-2-hydroxypropyl] (phenylmethyl)phosphinic acid hydrochloride (CGP58845; 5 μM) were added to block NMDA, non-NMDA, GABA A, and GABA B receptors, respectively. The internal solution (K-gluconate) was composed of (in mM) 126 K gluconate, 4 NaCl, 1 $MgSO_4$, 0.02 $CaCl_2$, 0.1 BAPTA, 15 glucose, 5 Hepes, 3 ATP, and 0.1 GTP (pH 7.3 with KOH). mPSCs were recorded in voltage-clamp configuration in the presence of TTX (300 nM) in the extracellular solution to block the generation and propagation of spontaneous action potentials. For excitatory transmission, D-AP5 (50 mM), BIC (30 mM) and CGP58845 (5 mM) were added to block NMDA, $GABA_A$, and $GABA_B$ receptors, respectively. D-AP5 (50 mM) and CNQX (10 mM) were added to block NMDA and non-NMDA, respectively for inhibitory transmission. The miniature PSC frequency, amplitude, and kinetics (synaptic charge, rise and decay time) were calculated using a peak detector function and analyzed using the MiniAnalysis (Synaptosoft) and Prism (GraphPad Software, Inc.) softwares. Spontaneous action potentials were recorded in current-clamp configuration at the resting membrane potential. Cells were maintained in Tyrode solution in the absence of synaptic transmission blockers. Action potentials were detected using an event detector function of Clampfit 10.7 (Molecular Devices, Sunnyvale, CA) software. All the reagents were bought by Tocris, otherwise specified in detail.

Supporting Information

Supporting Information is available from the Wiley Online Library or from the author.

Acknowledgements

A. Mehilli, D. Moruzzo, R. Ciancio, and I. Dallorto are gratefully acknowledged for primary cell culture preparations, as well as for technical and administrative support. This work was supported by the European Union's Horizon 2020 Research and Innovation Programme under Grant Agreement Grant Agreement No. 785219—Graphene Flagship—Core2 and Ministero degli Affari Esteri e Cooperazione Internazionale of Italy (Farnesina – MAECI) (Grant No. EPNZ0082). M.B. acknowledges supports from the EU Graphene Flagship-Core2 (Grant Agreement No. 785219) and the MSCA-COFUND Athenea3i scheme under the Grant Agreement No. 754446. J.S. acknowledges the support of the grant by the KIST Institution Programs (2Z06030, 2K02420). Y.L. and K.K. acknowledge support from the Institute for Basic Science (IBS-R026-D1). G.H.L. acknowledges supports from Basic Science Research Program and the International Research & Development Program through the NRF of Korea (2016M3A7B4910940, 2019K1A3A1A25000267) and Creative-Pioneering Researchers Program through Seoul National University (SNU). A.C. acknowledges the support of the European Union's Horizon 2020 research and innovation program under the Marie Skłodowska–Curie grant agreement No. 713640.

Conflict of Interest

The authors declare no conflict of interest.

Author Contributions

M.M. and J.-Y.L. contributed equally to this work. The manuscript was written through contributions of all authors. All authors have given approval to the final version of the manuscript.

Keywords

2D materials, hydrogenation, hydrophilicity, neurons, poly(ethylene terephthalate)

Received: July 2, 2020
Revised: October 27, 2020
Published online:

[1] S. J. Enna, M. Williams, *J. Pharmacol. Exp. Ther.* **2009**, *329*, 404.
[2] J. J. Danon, T. A. Reekie, M. Kassiou, *Trends Chem.* **2019**, *1*, 612.
[3] L. A. Bors, F. Erdö, *Sci. Pharm.* **2019**, *87*, 6.
[4] G. Orive, E. Anitua, J. L. Pedraz, D. F. Emerich, *Nat. Rev. Neurosci.* **2009**, *10*, 682.
[5] K. T. Nguyen, M. N. Pham, T. Van Vo, W. Duan, P. H.-L. Tran, T. T.-D. Tran, *Curr. Drug Metab.* **2017**, *18*, 786.
[6] M. E. Spira, A. Hai, *Nat. Nanotechnol.* **2013**, *8*, 83.
[7] D. Benninger, M. Schüpbach, *Ther. Umsch.* **2018**, *75*, 425.
[8] S. Picaud, J. A. Sahel, *C. R. Biol.* **2014**, *337*, 214.
[9] M. R. Antognazza, M. Di Paolo, D. Ghezzi, M. Mete, S. Di Marco, J. F. Maya-Vetencourt, R. Maccarone, A. Desii, F. Di Fonzo,

M. Bramini, A. Russo, L. Laudato, I. Donelli, M. Cilli, G. Freddi, G. Pertile, G. Lanzani, S. Bisti, F. Benfenati, *Adv. Healthcare Mater.* **2016**, *5*, 2271.
[10] N. G. Hatsopoulos, J. P. Donoghue, *Annu. Rev. Neurosci.* **2009**, *32*, 249.
[11] E. F. Chang, *Neuron* **2015**, *86*, 68.
[12] K. S. Novoselov, A. K. Geim, S. V. Morozov, D. Jiang, Y. Zhang, S. V. Dubonos, I. V. Grigorieva, A. A. Firsov, *Science* **2004**, *306*, 666.
[13] S. J. Dong, S. J. Guo, *Chem. Soc. Rev.* **2011**, *40*, 2644.
[14] A. K. Geim, *Science* **2009**, *324*, 1530.
[15] K. S. Novoselov, V. I. Fal'ko, L. Colombo, P. R. Gellert, M. G. Schwab, K. Kim, *Nature* **2012**, *490*, 192.
[16] A. Capasso, A. E. E. Del Rio Castillo, H. Sun, A. Ansaldo, V. Pellegrini, F. Bonaccorso, *Solid State Commun.* **2015**, *224*, 53.
[17] A. Capasso, S. Bellani, A. L. Palma, L. Najafi, A. E. Del Rio Castillo, N. Curreli, L. Cina, V. Miseikis, C. Coletti, G. Calogero, V. Pellegrini, A. Di Carlo, F. Bonaccorso, *2D Mater.* **2019**, *6*, 3.
[18] G. Reina, J. M. Gonzalez-Dominguez, A. Criado, E. Vazquez, A. Bianco, M. Prato, *Chem. Soc. Rev.* **2017**, *46*, 4400.
[19] D. McManus, S. Vranic, F. Withers, V. Sanchez-Romaguera, M. Macucci, H. Yang, R. Sorrentino, K. Parvez, S.-K. Son, G. Iannaccone, K. Kostarelos, G. Fiori, C. Casiraghi, *Nat. Nanotechnol.* **2017**, *12*, 343.
[20] B. M. L. Blaschke, S. Drieschner, A. Bonaccini Calia, K. Stoiber, L. Rousseau, G. Lissourges, J. A. Garrido, *2D Mater.* **2016**, *3*, 25007.
[21] E. Masvidal-Codina, X. Illa, M. Dasilva, A. B. Calia, T. Dragojević, E. E. Vidal-Rosas, E. Prats-Alfonso, J. Martínez-Aguilar, J. M. De la Cruz, R. Garcia-Cortadella, P. Godignon, G. Rius, A. Camassa, E. Del Corro, J. Bousquet, C. Hébert, T. Durduran, R. Villa, M. V. Sanchez-Vives, J. A. Garrido, A. Guimerà-Brunet, *Nat. Mater.* **2018**, *18*, 280.
[22] F. Veliev, Z. Han, D. Kalita, A. Briançon-Marjollet, V. Bouchiat, C. Delacour, *Front. Neurosci.* **2017**, *11*, 466.
[23] B. M. Blaschke, N. Tort-Colet, A. Guimerà-Brunet, J. Weinert, L. Rousseau, A. Heimann, S. Drieschner, O. Kempski, R. Villa, M. V. Sanchez-Vives, J. A. Garrido, *2D Mater.* **2017**, *4*, 2.
[24] N. P. Pampaloni, M. Lottner, M. Giugliano, A. Matruglio, F. D'Amico, M. Prato, J. A. Garrido, L. Ballerini, D. Scaini, *Nat. Nanotechnol.* **2018**, *13*, 755.
[25] K. E. Kitko, T. Hong, R. M. Lazarenko, D. Ying, Y. Q. Xu, Q. Zhang, *Nat. Commun.* **2018**, *9*, 796.
[26] A. Fabbro, D. Scaini, V. Leon, E. Vazquez, G. Cellot, G. Privitera, L. Lombardi, F. Torrisi, F. Tomarchio, F. Bonaccorso, S. Bosi, A. C. Ferrari, L. Ballerini, M. Prato, *ACS Nano* **2016**, *10*, 615.
[27] M. Chiacchiaretta, M. Bramini, A. Rocchi, A. Armirotti, E. Giordano, E. Vázquez, T. Bandiera, S. Ferroni, F. Cesca, F. Benfenati, *Nano Lett.* **2018**, *18*, 5827.
[28] M. Bramini, M. Chiacchiaretta, A. Armirotti, A. Rocchi, D. D. Kale, C. Martin, E. Vázquez, T. Bandiera, S. Ferroni, F. Cesca, F. Benfenati, *Small* **2019**, *15*, 1900147.
[29] M. Bramini, S. Sacchetti, A. Armirotti, A. Rocchi, E. Vázquez, V. León Castellanos, T. Bandiera, F. Cesca, F. Benfenati, *ACS Nano* **2016**, *10*, 7154.
[30] R. Rauti, N. Lozano, V. Leon, D. Scaini, M. Musto, I. Rago, F. P. Ulloa Severino, A. Fabbro, L. Casalis, E. Vazquez, K. Kostarelos, M. Prato, L. Ballerini, *ACS Nano* **2016**, *10*, 4459.
[31] R. Rauti, M. Medelin, L. Newman, S. Vranic, G. Reina, A. Bianco, M. Prato, K. Kostarelos, L. Ballerini, *Nano Lett.* **2019**, *19*, 2858.
[32] D. R. Nisbet, S. Pattanawong, J. Nunan, W. Shen, M. K. Horne, D. I. Finkelstein, J. S. Forsythe, *J. Colloid Interface Sci.* **2006**, *299*, 647.
[33] B. Li, Y. Ma, S. Wang, P. M. Moran, *Biomaterials* **2005**, *26*, 4956.
[34] J. Rafiee, X. Mi, H. Gullapalli, A. V. Thomas, F. Yavari, Y. Shi, P. M. Ajayan, N. A. Koratkar, *Nat. Mater.* **2012**, *11*, 217.
[35] F. Taherian, V. Marcon, N. F. A. Van Der Vegt, F. Leroy, *Langmuir* **2013**, *29*, 1457.
[36] P. Wick, A. E. Louw-Gaume, M. Kucki, H. F. Krug, K. Kostarelos, B. Fadeel, K. A. Dawson, A. Salvati, E. Vazquez, L. Ballerini, M. Tretiach, F. Benfenati, E. Flahaut, L. Gauthier, M. Prato, A. Bianco, *Angew. Chem., Int. Ed. Engl.* **2014**, *53*, 7714.
[37] S. Syama, P. V. Mohanan, *Nano-Micro Lett.* **2019**, *11*, 6.
[38] A. Capasso, T. Dikonimos, F. Sarto, A. Tamburrano, G. De Bellis, M. S. M. S. Sarto, G. Faggio, A. Malara, G. Messina, N. Lisi, *Beilstein J. Nanotechnol.* **2015**, *6*, 2028.
[39] N. Lisi, F. Buonocore, T. Dikonimos, E. Leoni, G. Faggio, G. Messina, V. Morandi, L. Ortolani, A. Capasso, *Thin Solid Films* **2014**, *571*, 139.
[40] N. Lisi, T. Dikonimos, F. Buonocore, M. Pittori, R. Mazzaro, R. Rizzoli, S. Marras, A. Capasso, *Sci. Rep.* **2017**, *7*, 9927.
[41] B. Deng, Z. Liu, H. Peng, *Adv. Mater.* **2019**, *31*, 1800996.
[42] F. Cesca, T. Limongi, A. Accardo, A. Rocchi, M. Orlando, V. Shalabaeva, E. Di Fabrizio, F. Benfenati, *RSC Adv.* **2014**, *4*, 45696.
[43] P. Roach, T. Parker, N. Gadegaard, M. R. Alexander, *Surf. Sci. Rep.* **2010**, *65*, 145.
[44] J. Son, S. Lee, S. J. Kim, B. C. Park, H.-K. Lee, S. Kim, J. H. Kim, B. H. Hong, J. Hong, *Nat. Commun.* **2016**, *7*, 13261.
[45] J. Son, N. Buzov, S. Chen, D. Sung, H. Ryu, J. Kwon, S. P. Kim, S. Namiki, J. Xu, S. Hong, K. Watanabe, T. Taniguchi, W. P. King, G. H. Lee, A. M. van der Zande, *Adv. Mater.* **2019**, *31*, 1903424.
[46] J. Son, J.-Y. Lee, N. Han, J. Cha, J. Choi, J. Kwon, S. Nam, K.-H. Yoo, G.-H. Lee, J. Hong, *Nano Lett.* **2020**, *20*, 5625.
[47] N. Li, X. Zhang, Q. Song, R. Su, Q. Zhang, T. Kong, L. Liu, G. Jin, M. Tang, G. Cheng, *Biomaterials* **2011**, *32*, 9374.
[48] M. Tang, Q. Song, N. Li, Z. Jiang, R. Huang, G. Cheng, *Biomaterials* **2013**, *34*, 6402.
[49] F. Veliev, A. Briançon-Marjollet, V. Bouchiat, C. Delacour, *Biomaterials* **2016**, *86*, 33.
[50] Z. He, S. Zhang, Q. Song, W. Li, D. Liu, H. Li, M. Tang, R. Chai, *Colloids Surf., B* **2016**, *146*, 442.
[51] D. W. Park, A. A. Schendel, S. Mikael, S. K. Brodnick, T. J. Richner, J. P. Ness, M. R. Hayat, F. Atry, S. T. Frye, R. Pashaie, S. Thongpang, Z. Ma, J. C. Williams, *Nat. Commun.* **2014**, *5*, 5258.
[52] D. W. Park, J. P. Ness, S. K. Brodnick, C. Esquibel, J. Novello, F. Atry, D. H. Baek, H. Kim, J. Bong, K. I. Swanson, A. J. Suminski, K. J. Otto, R. Pashaie, J. C. Williams, Z. Ma, *ACS Nano* **2018**, *12*, 148.
[53] M. Thunemann, Y. Lu, X. Liu, K. Kllç, M. Desjardins, M. Vandenberghe, S. Sadegh, P. A. Saisan, Q. Cheng, K. L. Weldy, H. Lyu, S. Djurovic, O. A. Andreassen, A. M. Dale, A. Devor, D. Kuzum, *Nat. Commun.* **2018**, *9*, 2035.
[54] M. L. DiFrancesco, E. Colombo, E. D. Papaleo, G. Manfredi, G. Lanzani, F. Benfenati, *Carbon* **2020**, *162*, 308.
[55] P. T. DeLassus, N. F. Whiteman, *Polymer Handbook*, 4th ed., Wiley, New York **1999**.
[56] R. Hiorns, *Polym. Int.* **2000**, *49*, 807.
[57] G. Orlando, *Regenerative Medicine Applications in Organ Transplantation*, 1st ed., Elsevier, New York **2014**.
[58] X. Li, Y. Zhu, W. Cai, M. Borysiak, B. Han, D. Chen, R. D. Piner, L. Colombo, R. S. Ruoff, L. Colomba, R. S. Ruoff, *Nano Lett.* **2009**, *9*, 4359.
[59] T. Miyamoto, S. -i Takahashi, H. Ito, H. Inagaki, Y. Noishiki, *J. Biomed. Mater. Res.* **1989**, *23*, 125.
[60] O. A. Adeleke, *Int. J. Pharm.: X* **2019**, *1*, 100023.
[61] M. C. Wang, W. P. Moestopo, S. Takekuma, S. F. Barna, R. T. Haasch, S. Nam, *J. Mater. Chem. C* **2017**, *5*, 11226.
[62] Y. Hao, Y. Wang, L. Wang, Z. Ni, Z. Wang, R. Wang, C. K. Koo, Z. Shen, J. T. L. Thong, *Small* **2010**, *6*, 195.
[63] D. Haberer, C. E. Giusca, Y. Wang, H. Sachdev, A. V. Fedorov, M. Farjam, S. A. Jafari, D. V. Vyalikh, D. Usachov, X. Liu, U. Treske, M. Grobosch, O. Vilkov, V. K. Adamchuk, S. Irle, S. R. P. Silva, M. Knupfer, B. Büchner, A. Grüneis, *Adv. Mater.* **2011**, *23*, 4497.

[64] K. Adachi, T. Yamada, H. Ishizuka, M. Oki, S. Tsunogae, N. Shimada, O. Chiba, T. Orihara, M. Hidaka, T. Hirokawa, M. Odagi, K. Konoki, M. Yotsu-Yamashita, K. Nagasawa, *Chem. - Eur. J.* **2020**, *26*, 2025.
[65] H. Liu, Y. Liu, D. Zhu, *J. Mater. Chem.* **2011**, *21*, 3335.
[66] Y. Du, Y. Li, T. Wu, *RSC Adv.* **2017**, *7*, 41838.
[67] L. Tang, N. Y. Lee, *Lab Chip* **2010**, *10*, 1274.
[68] Z. Chen, Y. Qi, X. Chen, Y. Zhang, Z. Liu, *Adv. Mater.* **2019**, *31*, 1803639.
[69] S. Kumar, S. H. Parekh, *Commun. Chem.* **2020**, *3*, 8.
[70] G. Cellot, E. Cilia, S. Cipollone, V. Rancic, A. Sucapane, S. Giordani, L. Gambazzi, H. Markram, M. Grandolfo, D. Scaini, F. Gelain, L. Casalis, M. Prato, M. Giugliano, L. Ballerini, *Nat. Nanotechnol.* **2009**, *4*, 126.
[71] R. A. Fischer, Y. Zhang, M. L. Risner, D. Li, Y. Xu, R. M. Sappington, *Adv. Healthcare Mater.* **2018**, *7*, 1701290.
[72] Z. Q. Feng, K. Yan, C. Shi, X. Xu, T. Wang, R. Li, W. Dong, J. Zheng, *Mater. Sci. Eng., C* **2018**, *90*, 685.
[73] C. F. Stevens, J. H. Williams, *J. Neurophysiol.* **2007**, *98*, 3221.
[74] O. Akhavan, E. Ghaderi, E. Abouei, S. Hatamie, E. Ghasemi, *Carbon* **2014**, *66*, 395.
[75] J. E. Lee, G. Ahn, J. Shim, Y. S. Lee, S. Ryu, *Nat. Commun.* **2012**, *3*, 1024.
[76] Y. J. Yu, G. H. Lee, J. Il Choi, Y. S. Shim, C. H. Lee, S. J. Kang, S. Lee, K. T. Rim, G. W. Flynn, J. Hone, Y. H. Kim, P. Kim, C. Nuckolls, S. Ahn, *Adv. Mater.* **2017**, *29*, 1603925.
[77] A. L. Jørgensen, D. A. Duncan, C. F. P. Kastorp, L. Kyhl, Z. Tang, A. Bruix, M. Andersen, B. Hammer, T. L. Lee, L. Hornekær, R. Balog, *Phys. Chem. Chem. Phys.* **2019**, *21*, 13462.
[78] Y. Cho, J.-M. Yang, D. Van Lam, S.-M. Lee, J.-H. Kim, K.-Y. Han, J. Chang, *Appl. Microsc.* **2014**, *44*, 133.